Spin-Flip and Element-Sensitive Electron Scattering in the $BiAg_2$ Surface Alloy

S. Schirone,[1] E. E. Krasovskii,[2,3,4] G. Bihlmayer,[5] R. Piquerel,[1] P. Gambardella,[1,6,7] and A. Mugarza[1]
[1]*ICN2-Institut Catala de Nanociencia i Nanotecnologia, Campus UAB, 08193 Bellaterra, Barcelona, Spain*
[2]*Departamento de Física de Materiales, Facultad de Ciencias Químicas, Universidad del Pais Vasco/Euskal Herriko Unibertsitatea, Apartado 1072, San Sebastián/Donostia, 20080 Basque Country, Spain*
[3]*Donostia International Physics Center (DIPC), Paseo Manuel de Lardizabal 4, San Sebastián/Donostia, 20018 Basque Country, Spain*
[4]*IKERBASQUE, Basque Foundation for Science, 48011 Bilbao, Spain*
[5]*Peter Grünberg Institut and Institute for Advanced Simulation, Forschungszentrum Jülich and JARA, 52425 Jülich, Germany*
[6]*Institució Catalana de Recerca i Estudis Avancats (ICREA), E-08193 Barcelona, Spain*
[7]*Department of Materials, ETH Zurich, Hönggerbergring 64, CH-8093 Zurich, Switzerland*
(Received 28 August 2014; published 22 April 2015)

Heavy metal surface alloys represent model systems to study the correlation between electron scattering, spin-orbit interaction, and atomic structure. Here, we investigate the electron scattering from the atomic steps of monolayer $BiAg_2$ on Ag(111) using quasiparticle interference measurements and density functional theory. We find that intraband transitions between states of opposite spin projection can occur via a spin-flip backward scattering mechanism driven by the spin-orbit interaction. The spin-flip scattering amplitude depends on the chemical composition of the steps, leading to total confinement for pure Bi step edges, and considerable leakage for mixed Bi-Ag step edges. Additionally, the different localization of the occupied and unoccupied surface bands at Ag and Bi sites leads to a spatial shift of the scattering potential barrier at pure Bi step edges.

DOI: 10.1103/PhysRevLett.114.166801 PACS numbers: 73.20.At, 71.70.Ej, 68.37.Ef

The spin-orbit interaction (SOI) can dramatically influence electron scattering on the surface of crystalline compounds. A most striking consequence is the quenching of backscattering, which arises from the entanglement between the spin and crystal momentum in the surface states of topological insulators and other two-dimensional systems [1–3]. The absence of backscattering makes an electric current less sensitive to defects and facilitates the generation of spin currents, which is attractive for applications in spintronics [4–7].

The effect of the SOI at the surface, where the spatial inversion symmetry is broken, can be qualitatively modeled by the Rashba-Bychkov Hamiltonian. This model predicts fully in-plane, chirally polarized surface states [8,9]. Although conventional Rashba-type paradigmatic examples exist, such as Au(111) [9,10], the spin texture in real materials is, in general, more complex. A strong in-plane scattering by the periodic crystal lattice leads to an entangled spin-orbital structure of the Bloch states with a finite out-of-plane spin component [11] and, at the same time, reduces the spin polarization in the $\mathbf{k}_{\parallel} \times \mathbf{z}$ direction ($\mathbf{z}$: perpendicular to surface plane) [12]. These deviations from the Rashba-type spin texture must be taken into account for the correct understanding of the scattering mechanism in real solids [13].

Far from the conventional Rashba-type system, heavy element (X), ordered XAg_2 surface alloys grown on Ag(111) represent an ideal case to study the effect of the spin texture on electron scattering. Out-of-plane spin components have been observed in these alloys [12], for which theory predicts a complex in-plane spin texture of varying polarization that substantially deviates from the conventional Rashba spin splitting [14,15]. Previous investigations of the $BiAg_2$ alloy showed evidence of electron backscattering for both the occupied and unoccupied surface bands [16,17]. However, these results were interpreted in the framework of spin-conserving scattering within fully spin-polarized Rashba-type bands, disregarding the radically different spin texture described by *ab initio* band structure calculations, where the spin polarization of each branch of the unoccupied band is significantly less than 100% and of opposite sign [see Fig. 3(a)]. With this spin-orbit texture, a new SOI-driven spin-flip mechanism can emerge, as recently suggested [18].

In this Letter, we provide experimental evidence of SOI-driven spin-flip scattering from monoatomic steps of the $BiAg_2$ surface alloy. By analyzing the quasiparticle interference (QPI) patterns produced by atomically straight steps with different concentrations of Ag and Bi atoms, we quantify the transmission and reflection coefficients for electrons impinging on heterogeneous scatterers. Additionally, we find that the stronger SOI at the heavy metal sites and the element-specific localization of the occupied and unoccupied surface states lead to substantial differences in the scattering amplitudes and phase shifts.

The experiments were performed using a scanning tunneling microscope (STM) operated at 5 K in ultrahigh vacuum. The Ag(111) single crystal was cleaned by cycles

of Ar^+ bombardment and annealing at 800 K. The $BiAg_2$ surface alloy was grown *in situ* by evaporating 1/3 of a monolayer of Bi from a Knudsen cell with the sample kept at 400 K and at a pressure $p < 2 \times 10^{-10}$ mBar. Spectroscopic (STS) measurements were performed by using the lock-in technique, with a bias voltage modulation of frequency 3 kHz and amplitude 3 mV_{rms}. The spin and orbital texture of one side of a structurally relaxed, symmetric $\sqrt{3} \times \sqrt{3}$ $BiAg_2/Ag(111)$ film is analyzed based on density functional theory using the generalized gradient approximation and full-potential linearized augmented plane-wave method, as described in Ref. [14].

We investigated scattering from two different step types, perpendicular to the ΓM and ΓK directions, labeled as A and B hereafter. A steps have the highest density of Bi atoms and follow the close-packed direction of the surface alloy. This is the preferred step direction on this surface. To study scattering from B steps, we deliberately crashed the surface with the STM tip. Dislocation lines created by the crash propagate along the close-packed direction of bulk Ag, rotated by 30° with respect to that of the surface alloy, and appear on the surface as straight, kinkless steps. Figure 1(a) shows a topographic image with the two types of steps. Since only Bi atoms are imaged by STM [19], the atomic resolution allows us to resolve the composition of each step edge, as depicted in the schematic models in Fig. 1(b).

The scattering vectors $q(E)$ are obtained from the periodicity of QPI patterns by performing the spatial Fourier transformation (FT) of a set of dI/dV spectra (FT-STS) acquired in the direction perpendicular to the steps. For bands with circular isoenergy contours such as those of $BiAg_2$, QPI are dominated by 180° backscattering events, and hence, the wave vectors $q = |\mathbf{k}_f - \mathbf{k}_i|$ can be directly assigned to transitions between initial and final states ($\mathbf{k}_{i,f}$) in the direction perpendicular to the steps. Figure 2(a) shows an example of a set of spectra acquired along a line crossing two A steps, indicated on the top image. The dI/dV intensity, plotted in color scale, has been normalized by subtraction of a reference spectrum acquired away from scatterers in order to enhance the interference features [20,21]. In terraces larger than the electron coherence length, the QPI patterns arising from the occupied and unoccupied $BiAg_2$ bands form Friedel-like oscillations in the continuum density of states (DOS). This is shown in the left terrace of Fig. 2(a). In smaller terraces the QPI are quantized due to the coherent scattering from steps at both sides, as shown in the center and right terraces in Fig. 2(a). The two q branches identified in the FT-STS of Fig. 2(b), one for each surface band, are labeled D_1 and D_2 in agreement with those measured in Ref. [16]. The q vectors are then compared to transitions within the calculated band structure by linking pairs of initial and final states, as shown in Fig. 2(c) [24]. The agreement between q vectors and intraband transitions within both unoccupied and occupied bands indicates that this is the main scattering channel.

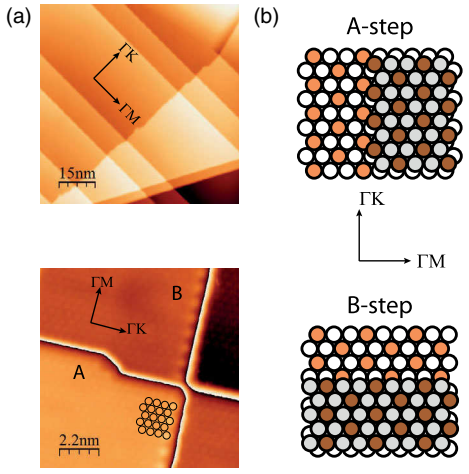

FIG. 1 (color online). (a) Monoatomic steps perpendicular to the ΓM (A) and ΓK (B) directions. The atomically resolved image (bottom) shows the Bi sites as protrusions. Set point: $I = 0.59$ nA, $V_b = 1000$ mV (top) and 28 mV (bottom). (b) Atomic structure of the different step edges derived from the images in (a). Bi atoms of the lower (upper) terrace correspond to orange (brown) circles, and Ag atoms to white (grey) circles, respectively.

Figure 2(c) shows that, in the energy range of the unoccupied band, the q vectors connect states within the same band but opposite spin polarization. These intraband transitions would be forbidden if the states were fully spin-polarized and if no spin-flip scattering processes were allowed [25]. The spin and orbital decomposition of the calculated band structure, however, reveals a more complex scenario. The spin-polarization of the states in the unoccupied $BiAg_2$ band is, at most, 75%, as shown in Fig. 3(a). The reduced spin polarization is not accompanied by a significant out-of-plane spin component, but results from a mixture of oppositely in-plane polarized p_x and p_y orbitals. This is shown in Fig. 3(b) in real space and in Fig. 3(c) in k space. Mixing the orbital character is facilitated in the scattering process by the spin-orbit interaction term $\mathbf{L} \cdot \mathbf{S}$, which allows electron scattering from a p_y orbital with spin in the $+x$ direction into a p_x orbital with spin in the $-x$ direction [27,28]. The electron reflection from the step, therefore, involves the scattering between p_x and p_y orbitals of opposite spin. Similar orbital decompositions have been observed in the $BiCu_2$ [15] and $PbAg_2$ [18], suggesting that spin-flip scattering is a general feature of these surface alloys.

The comparison of QPIs formed by scattering at steps with different chemical composition provides us with an atomistic picture of the SOI-driven intraband scattering mechanism. The different intensity of simultaneously mapped QPI patterns arising from the two step edge types already indicates different scattering properties of A and B

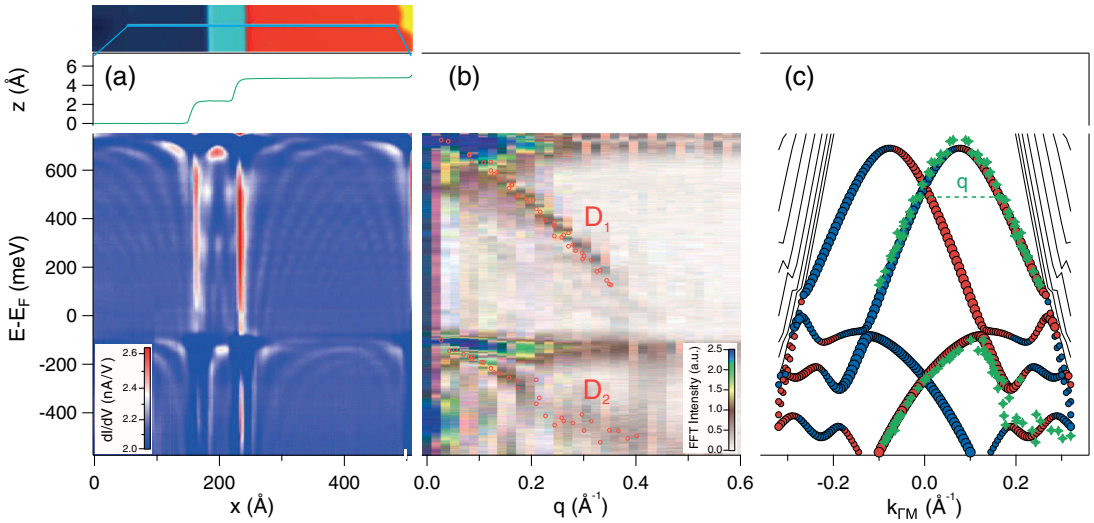

FIG. 2 (color online). Electron scattering from A steps. (a) dI/dV spectra acquired along a line crossing several steps (topography and line profile shown on top). Set point: $I = 1.6$ nA, $V_b = -2.0$ V. (b) Fourier transform of the dI/dV spectra along the x axis acquired on the left and right terraces. The scattering vectors q for the D_1 and D_2 branches are indicated as open red circles. (c) Comparison of the experimental scattering vectors and calculated band structure. The color and size of the points in the band structure correspond to the sign and magnitude of the spin polarization in the $\mathbf{k}_\parallel \times \mathbf{z}$ direction, respectively.

steps [21]. A more quantitative analysis of the scattering coefficients is carried out by fitting the spatial modulation of the quantized QPI formed in the smaller terraces with Fabry-Pérot resonances [21]. Reflection coefficients and phase shifts, which are univocally related to transmission, can be directly extracted from this fit.

We first focus on how the states in the same band scatter differently from each step type, as can be observed in Fig. 4(a). Figure 4(b) shows the case of the $N = 2$ resonance of the unoccupied band in this terrace. For the fit we use, $m_{\text{eff}} = -0.16 m_e$ and $E_0 = 731$ meV, obtained from the analysis of spectra acquired away from scatterers [21]. The region close to the steps is excluded from the fit due to the strong contribution of edge-related features [see Fig. 2(a)]. Outside this region, the experimental data nicely fit the Fabry-Pérot intensity for both step types. The resulting scattering coefficients are listed in Table I. Here, we comment on the asymmetry factor $R_{\text{as}} = (r_l - r_r)/(r_l + r_r)$, instead of the single reflection coefficients, which are more sensitive to fitting procedures. The small deviations found for R_{as} and $\phi_{l/r}$ for varying prefactor (ρ_s/π) values, listed in Table I, are indicative of the robustness of the fit [21]. For A steps, the reflection is strongly asymmetric, being larger in the downwards step direction $(r_l > r_r)$. In contrast, a rather symmetric phase shift close to $\pm\pi$ indicates that transmission is negligible at both sides. These results are similar to those reported for the Ag(111) surface state [20,23]. The results for B steps, however, are strikingly different. Both reflection and phase shift are symmetric, but $\phi_{l/r}$ strongly deviate from π, the value characterizing infinite barriers. This is an indication of a substantial transmission across B steps.

Next, we compare how states from the occupied and unoccupied bands scatter from the same step type. The spatial distribution of resonances of the occupied band deviate more strongly from the LDOS of the Fabry-Pérot model, probably due to the proximity of bulk Ag states [29]. Hence, we limit our analysis to the quantification of lateral shifts of the spatial distributions by comparing the

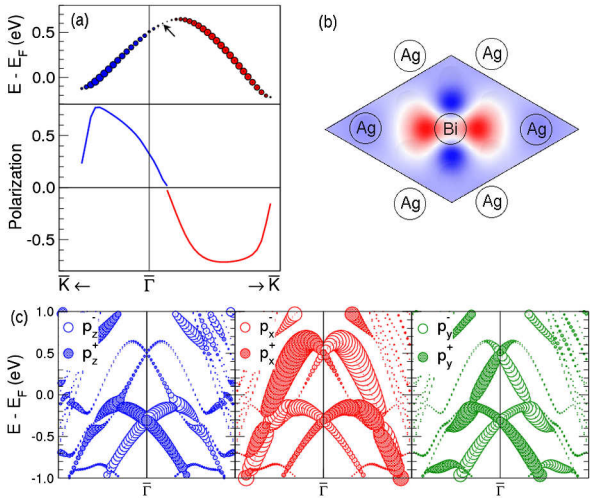

FIG. 3 (color online). (a) Dispersion and spin polarization for a selected branch of the unoccupied bands. (b) Spin density of the state marked by an arrow in (a). The cutting plane is chosen through the Bi atom, in the center of the unit cell. (c) Orbital-resolved band structure along ΓK. The size of the symbols indicates the Bi p_z (left), p_x (middle), and p_y (right) contribution to the state. Opposite spin directions are shown by full and empty symbols. Similar results are obtained for the ΓM direction.

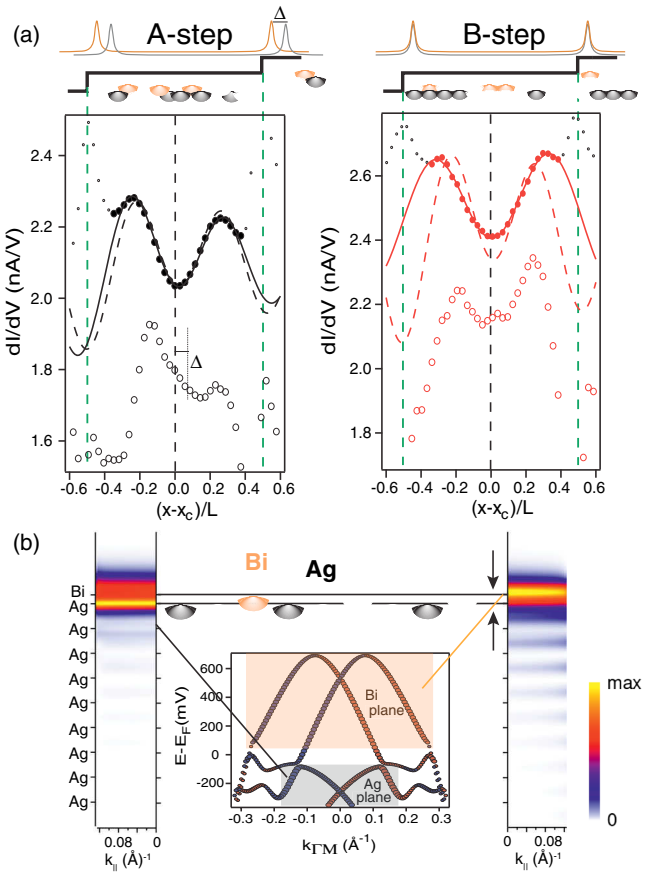

FIG. 4 (color online). (a) $dI/dV(x)$ for the $N = 2$ resonance of the unoccupied (closed symbols) and occupied band (open symbols) for resonators of the two step types ($L = 70$ Å for A type, and 75 Å for B type). The fit of the unoccupied state with Fabry-Pérot resonances is shown for free $\phi_{l,r}$ (solid line) and fixed $\phi_{l,r} = -\pi$ (dashed line) [21]. The center of the terrace (x_c) and step edges are indicated by black and green vertical dashed lines, respectively. The step direction, atomic arrangement, and potential barriers are sketched on top. (b) DOS(z) integrated over the z = constant plane parallel to the surface for the two surface states, calculated using the method of Ref. [30].

position of the maxima of the $N = 2$ resonance in each band. For A-type resonators, the maxima are shifted by $\Delta = 3 \pm 1$ Å to the right. We find similar values, within the error bar, for terrace sizes ranging from 70 to 179 Å, thereby excluding any effect related to an asymmetric transmission, which should be proportional to L [23]. In contrast, the resonances of the occupied and unoccupied bands are aligned at the center of B-type resonators. A similar analysis with the $N = 1$ resonances leads to the same conclusions [21].

We attribute the different scattering behavior of each step type to the element-specific localization of wave functions on the $BiAg_2$ bilayer, as shown in Fig. 4(c) by the depth profile of the density of occupied and unoccupied surface states. Unoccupied states are strongly localized on the Bi plane, whereas occupied states are mainly on Ag.

TABLE I. Reflection coefficients, asymmetry factor and phase shifts obtained from the fitting of the $N = 2$ resonances of the unoccupied band, shown in Fig. 4(b). The error represents variations in the fit series of Fig. S3 [21].

	A step	B step
r_l	0.70 ± 0.30	0.40 ± 0.18
r_r	0.21 ± 0.07	0.36 ± 0.15
R_{as}	0.53 ± 0.04	-0.06 ± 0.01
ϕ_l/π	-0.83 ± 0.02	-0.56 ± 0.02
ϕ_r/π	-0.95 ± 0.02	-0.51 ± 0.02

This makes electrons sensitive to the chemical composition of the steps.

For the unoccupied states, their localization on the heavy Bi atoms favors the $\mathbf{L} \cdot \mathbf{S}$ perturbation required for the spin flip scattering, making this SOI-driven scattering mechanism more efficient in barriers with higher concentration of Bi atoms (A steps) than in the regions where Bi and Ag are mixed (B steps). This suggests a connection between the SOI strength in the scattering region and the probability of backscattering that is consistent with the phase shifts reported in Table I. The situation is qualitatively different for the occupied states, which are localized more on the Ag side of the surface alloy and have a different orbital character. In this case, spin conserving scattering can account for the observed intraband transitions [see Fig. 3(c)].

The localization of occupied and unoccupied states in different elements leads to an additional effect: if pure Bi and Ag atomic rows alternate parallel to the steps, as in the case of A steps, the step potential barrier for each band will appear laterally shifted by one atomic row, in agreement with the data in Fig. 4(b). We note that the observed shift of the occupied resonance towards the direction of the upward step indicates that the first atomic row at the A-step edge is composed of Bi atoms, as schematically represented in Fig. 4(b), and in agreement with the step edge structure proposed in Fig. 1(b). Here, we discard any effect related to the different spin and orbital composition of the two bands, since these are isotropic, and hence, similar effects should be expected in both types of resonators (see Fig. S6 in Ref. [21]).

In summary, we identified a backscattering spin-flip mechanism that is not predicted in the usual framework of Rashba-type surface states. This involves the scattering between p orbitals with opposite spin polarization, and is induced by the same SOI that gives rise to the entangled spin-orbital texture of the surface states. This scattering mechanism is highly sensitive to the chemical composition of the step edges due to the different degree of localization of the occupied and unoccupied electronic wave functions on Ag and Bi sites. By utilizing parallel steps as Fabry-Pérot resonators, we derived the scattering coefficients for different step types and found that spin-flip scattering can lead to total confinement for pure Bi step edges, but considerable leakage for mixed Bi-Ag step edges.

The correlation of the scattering properties with the atomic scale chemical composition of the steps allows us to set a connection between the SOI strength in the scattering region and the probability of backscattering. We also show that the respective localization of occupied and unoccupied bands on the Ag and Bi planes of the $BiAg_2$ bilayer leads to shifted element-specific potential barriers for steps consisting of alternate Bi and Ag rows. These results can be generalized to other heterogeneous heavy metal compounds with strong Rashba interaction, and are relevant for engineering electron confinement in these materials.

We acknowledge support from the Spanish Ministerio de Ciencia e Innovación (Grants No. MAT2010-15659 and No. MAT2013-46593-C6-5-P and No. FIS2013-48286-C2-1-P), the Swiss National Science Foundation (Grant No. 200021-153404), and Agència de Gestió d'Ajuts Universitaris i de Recerca (Grant No. 2009 SGR 695). G. B. is grateful for computing time on the JUROPA supercomputer at the Jülich Supercomputing Centre (JSC).

[1] M. Franz, Nature (London) **466**, 323 (2010).
[2] P. Roushan, J. Seo, C. V. Parker, Y. S. Hor, D. Hsieh, D. Qian, A. Richardella, M. Z. Hasan, R. J. Cava, and A. Yazdani, Nature (London) **460**, 1106 (2009).
[3] J. I. Pascual, G. Bihlmayer, Y. M. Koroteev, H.-P. Rust, G. Ceballos, M. Hansmann, K. Horn, E. V. Chulkov, S. Blügel, P. M. Echenique, and P. Hofmann, Phys. Rev. Lett. **93**, 196802 (2004).
[4] D. Pesin and A. H. MacDonald, Nat. Mater. **11**, 409 (2012).
[5] I. M. Miron, K. Garello, G. Gaudin, P.-J. Zermatten, M. V. Costache, S. Auffret, S. Bandiera, B. Rodmacq, A. Schuhl, and P. Gambardella, Nature (London) **476**, 189 (2011).
[6] I. M. Miron, G. Gaudin, S. Auffret, B. Rodmacq, A. Schuhl, S. Pizzini, J. Vogel, and P. Gambardella, Nat. Mater. **9**, 230 (2010).
[7] J. C. R. Sánchez, L. Vila, G. Desfonds, S. Gambarelli, J. P. Attané, J. M. De Teresa, C. Magén, and A. Fert, Nat. Commun. **4**, 2944 (2013).
[8] Y. A. Bychkov and E. I. Rashba, JETP Lett. **39**, 78 (1984).
[9] J. Henk, M. Hoesch, J. Osterwalder, A. Ernst, and P. Bruno, J. Phys. Condens. Matter **16**, 7581 (2004).
[10] S. LaShell, B. A. McDougall, and E. Jensen, Phys. Rev. Lett. **77**, 3419 (1996).
[11] A. Takayama, T. Sato, S. Souma, and T. Takahashi, Phys. Rev. Lett. **106**, 166401 (2011).
[12] F. Meier, H. Dil, J. Lobo-Checa, L. Patthey, and J. Osterwalder, Phys. Rev. B **77**, 165431 (2008).
[13] E. E. Krasovskii, Phys. Rev. B **90**, 115434 (2014).
[14] G. Bihlmayer, S. Blügel, and E. V. Chulkov, Phys. Rev. B **75**, 195414 (2007).
[15] H. Mirhosseini, J. Henk, A. Ernst, S. Ostanin, C.-T. Chiang, P. Yu, A. Winkelmann, and J. Kirschner, Phys. Rev. B **79**, 245428 (2009).
[16] L. El-Kareh, P. Sessi, T. Bathon, and M. Bode, Phys. Rev. Lett. **110**, 176803 (2013).
[17] H. Hirayama, Y. Aoki, and C. Kato, Phys. Rev. Lett. **107**, 027204 (2011).
[18] L. El-Kareh, G. Bihlmayer, A. Buchter, H. Bentmann, S. Blügel, F. Reinert, and M. Bode, New J. Phys. **16**, 045017 (2014).
[19] C. R. Ast, G. Wittich, P. Wahl, R. Vogelgesang, D. Pacilé, M. C. Falub, L. Moreschini, M. Papagno, M. Grioni, and K. Kern, Phys. Rev. B **75**, 201401(R) (2007).
[20] J. E. Ortega, J. Lobo-Checa, G. Peschel, S. Schirone, Z. M. Abd El-Fattah, M. Matena, F. Schiller, P. Borghetti, P. Gambardella, and A. Mugarza, Phys. Rev. B **87**, 115425 (2013).
[21] See Supplemental Material at http://link.aps.org/supplemental/10.1103/PhysRevLett.114.166801, which includes Refs. [16,19,20,22,23].
[22] J. Seo, P. Roushan, H. Beidenkopf, Y. S. Hor, R. J. Cava, and A. Yazdani, Nature (London) **466**, 343 (2010).
[23] L. Bürgi, O. Jeandupeux, A. Hirstein, H. Brune, and K. Kern, Phys. Rev. Lett. **81**, 5370 (1998).
[24] The *ab initio* band structure has been shifted down in energy in order to obtain the best match with the experimental scattering vectors. For the symmetric unoccupied band, the data pair connected by the q vector has been centered with respect to the maxima. For the asymmetric unoccupied band, we plot the pair of data by associating the left one with the inner branch of the band.
[25] The question of interband scattering does not arise in the present experiment because it involves time-reversal partners, which do not produce interference patterns (see Appendix of Ref. [26]).
[26] L. Petersen and P. Hedegård, Surf. Sci. **459**, 49 (2000).
[27] H. Zhang, F. Freimuth, G. Bihlmayer, M. Ležaić, S. Blügel, and Y. Mokrousov, Phys. Rev. B **87**, 205132 (2013).
[28] S. Konschuh, M. Gmitra, and J. Fabian, Phys. Rev. B **82**, 245412 (2010).
[29] L. Vitali, P. Wahl, M. Schneider, K. Kern, V. Silkin, E. Chulkov, and P. Echenique, Surf. Sci. **523**, L47 (2003).
[30] E. E. Krasovskii, F. Starrost, and W. Schattke, Phys. Rev. B **59**, 10504 (1999).